METRICA
METRology Institutional CAtalog

ISTITUTO NAZIONALE DI RICERCA METROLOGICA
Repository Istituzionale

GISAXS Analysis of the In-Depth Morphology of Thick PS-b-PMMA Films

This is the author's submitted version of the contribution published as:

Original
GISAXS Analysis of the In-Depth Morphology of Thick PS-b-PMMA Films / Ferrarese Lupi, F., Giammaria, T.J., Seguini, G., Laus, M., Dubček, P., Pivac, B., Bernstorff, S., Perego, M.. - In: ACS APPLIED MATERIALS & INTERFACES. - ISSN 1944-8244. - 9:12(2017), pp. 11054-11063-11063. [10.1021/acsami.7b01366]

Availability:
This version is available at: 11696/56925 since: 2018-01-30T10:42:03Z

Publisher:
American Chemical Society

Published
DOI:10.1021/acsami.7b01366

Terms of use:

This article is made available under terms and conditions as specified in the corresponding bibliographic description in the repository

Publisher copyright
American Chemical Society (ACS)
Copyright © American Chemical Society after peer review and after technical editing by the publisher. To access the final edited and published work see the DOI above.

(Article begins on next page)

14 October 2026

GISAXS Analysis of the In-Depth Morphology of Thick PS-*b*-PMMA Films

Federico Ferrarese Lupi [1,2*], *Tommaso Jacopo Giammaria* [1,3], *Gabriele Seguini* [1], *Michele Laus* [3], *Pavo Dubček* [4], *Branko Pivac* [4], *Sigrid Bernstorff* [5], *Michele Perego*[1]

[1] *Laboratorio MDM, IMM-CNR, Via C. Olivetti 2, 20864 Agrate Brianza, Italy*

[2] *Nanoscience and Materials Division, Istituto Nazionale Ricerca Metrologica, Strada delle Cacce 91, 10135 Torino, Italy*

[3] *Dipartimento di Scienze e Innovazione Tecnologica (DISIT), Università del Piemonte Orientale ''A. Avogadro'', Viale T. Michel 11, 1512 Alessandria, Italy*

[4] *Institut Ruđer Bošković, Bijenička cesta 54, 10000 Zagreb, Croatia*

[5] *Elettra-Sincrotrone Trieste, SS 14, Km 163.5, in AREA Science Park, 34149 Basovizza (TS), Italy*

Corresponding author e-mail: f.ferrareselupi@inrim.it

KEYWORDS: Block Copolymers, GISAXS, PS-*b*-PMMA, Rapid Thermal Processing, Self-assembly

ABSTRACT

The morphological evolution of cylinder forming poly(styrene)-*b*-poly(methyl methacrylate) (PS-*b*-PMMA) block copolymers (BCPs) thick films treated at high temperatures in the Rapid Thermal Processing (RTP) machine was monitored by means of in-depth Grazing Incidence Small Angle X-ray Scattering (GISAXS). The use of this non-disruptive technique allowed revealing the formation of buried layers composed of both parallel and perpendicular oriented cylinders as a function of the film thickness ($24 \leq h \leq 840$ nm) and annealing time ($0 \leq t \leq 900$

s). Three distinct behaviors were observed depending on the film thickness. Up to $h \leq 160$ nm an homogeneous film consisting of perpendicularly oriented cylinders is observed. When h is comprised between 160 and 700 nm, a decoupling process between both the air-BCP and the substrate BCP interfaces takes place, leading to the formation of mixed orientations (parallel and perpendicular) of the cylinders. Finally for $h > 700$ nm, the two interfaces are completely decoupled and the formation of a superficial layer of about 50 nm composed of perpendicular cylinders was observed. Furthermore, the through film morphology affects the nanodomain long range order that substantially decreases in correspondence of the beginning of the decoupling process. By exposing the thick samples to longer thermal treatments an increase in the long range order of the nanodomains, without any sensible variation of the thickness of the superficial layer.

INTRODUCTION

The growing interest that block copolymers (BCPs) aroused as a versatile tool capable of generating well ordered structures at sub-20 nm scale has pushed the parallel need for a clear understanding of the dynamics of the self-assembly (SA) process. While there is a wide literature concerning the characterization of the in depth morphology in BCP films having a thickness (h) comparable to the characteristic dimensions of the nanometric domains[1] (i.e. center to center distance L_0 and diameter d), only few works are devoted to the characterization of thick films where $h >> L_0$.[2-3] However, the control over the orientation and long range ordering of the nano-domains in thick BCP films is mandatory for many practical applications in several technological fields, such as the fabrication of advanced lithographic masks, the realization of membranes for water purification,[4-5-6] drug delivery,[7] energy storage,[8-9-10] and the production of organic-

inorganic photovoltaic devices.[11-12-13] For all these applications, the capability to control both the orientation and the ordering of the nano-domains is crucial. The preferred orientation of the nano-domains required in most of the aforementioned technological applications is the one perpendicular with respect to the substrate. Several methods were developed to obtain the perpendicular orientation of the block copolymer features including the solvent vapor annealing,[14-15] the application of external electric fields,[16-17] or by tailoring the surface energy using a neutral brush layer.[18]

Prior to the application of the BCPs on large-scale production of nanostructured devices a number of challenges has to be addressed, such as the increase of the resistence of the film to etching processes, the reduction of the processing time, and the improvement of the uniformity of orientation and ordering of the nano-domains over wide areas. The intrinsic resistance of the BCP films to subsequent etching or deposition processes can be increased by selectively substituting one of the copolymer with an inorganic compound, using the *Sequential Infiltration Synthesis* technique (SIS).[19-20]

On the other hand, the issues concerning the reduction of the processing time and increase of the ordering can be overcome by performing fast treatments at high temperatures using for example the laser spike annealing approach[21] or the Rapid Thermal Processing (RTP) machine[22]. In this latter case, a simple thermal treatment by a machine commonly employed in the semiconductor industry, was demonstrated to be able to obtain highly uniform BCP masks having different characteristic dimensions[23-24] and morphologies[25,26].

Several investigations highlighted that the RTP annealing performances are critically dependent on the amount of solvent retained inside both the BCP and RCP films.[27,28,29]

The solvent was also recognized as responsible for some peculiar changes in phase and orientation of the domains occurring during the SA process.[30-31-32] Indeed, the solvent retained inside PS-*b*-PMMA thin films once treated at high temperatures with a fast heating rate increases the mobility of the polymeric chains thus enabling fast long-range ordering dynamics.[25] On the other hand the solvent is also the cause of unexpected effects, such as the formation of buried interfaces composed of cylindrical phase domains registered with the original lamellar pattern due to the preferential swelling of the PS,[27] or the orientational flipping of cylindrical domains confined inside periodic gratings.[33]

In this context, the understanding of the complex ordering and orientation processes occurring in thick BCP films exposed to high temperature thermal treatments is very challenging. The morphological analysis of the inner part of the BCP films is normally performed by means of disruptive processes such as lift-off or plasma etching. A recent study focused on the characterization of BCP films processed at high temperature in view of lithographic applications has been reported by our group for samples with thickness $h < 400$ nm.[34] In this study, we confirmed the formation of a perpendicular cylinder structure up to $h = 160$ nm. Above this value, a consistent reduction of the ordering at the cylinder domain surface was observed. However, the adopted lift-off technique does not provide extensive insights regarding the morphological changings occurring inside thick BCP films, thus the use of alternative methods such as the cross-sectional SEM analysis or TEM tomography[35] is requested. The main issue preventing a systematic use of this approach is that information can be obtained only at local scale. Accordingly, to probe the internal morphology and the orientation of the nanostructures on large-scale, alternative approaches are required. To this purpose, in the last years the Grazing Incidence Small-Angle X-ray Scattering (GISAXS) technique gained increasing importance

since it provides accurate information about the structural changes in SA BCP films simultaneously at large scale and at nanometric level.[36-37] In this work, the GISAXS technique was exploited to systematically study the internal morphology of RTP treated asymmetric BCP films with thickness up to 840 nm.

EXPERIMENTAL SECTION

Substrate neutralization

Silicon substrates, with ~1.8 nm thick native silicon dioxide (SiO_2) layer, were used as a support for the BCP SA. The substrates (~1 cm^2 surface) were treated with a Piranha solution at 80 °C for 40 min to eliminate any residual organic contamination and to increase the surface density of hydroxyl groups. The substrate neutralization was obtained with high temperature processes by grafting on the native SiO_2 an -OH terminated P(S-*r*-MMA) RCP with a styrene fraction 0.62, M_n = 13.5 kg·mol^{-1} and PDI = 1.26. A solution with 18 mg of P(S-*r*-MMA) in 2 ml of toluene was prepared in ultrasonic bath and spun on the substrates at 3000 rpm for 30 s. In order to induce the grafting process and to allow chain ends to diffuse and react with the substrate, the samples were RTP annealed in N_2 atmosphere at an annealing temperature of T_a = 250 °C for an overall processing time of t_a = 600 s.[34] The non-anchored chains were removed after annealing with a 300 s sonication bath in toluene. The thickness of the resulting layer was ~ 8 nm as detected by ellipsometry measurements.

Block copolymer deposition

The asymmetric PS-*b*-PMMA BCP with a styrene fraction of 0.71, M_n = 67.1 kg·mol^{-1} and PDI = 1.09 was purchased from Polymer Source Inc. and used without further purification. A solution with PS-*b*-PMMA in toluene was prepared. The BCP SA process was promoted by annealing the samples at T_a = 270 ° → io non lo evidenzierei... C for t_a = 300 s. The film thickness was tuned between 24 nm and 840 nm by changing the BCP concentration in the toluene solution. The samples are labeled in the following sections using the letter B followed by a number indicating the thickness of the sample expressed in nanometers (*i.e.*: B24, B100, B194, B350, B714, B840). In order to selectively remove the PMMA from the PS matrix the same pore opening process was performed on all the samples.[32] The main steps of the pore opening process consist in the exposure to ultraviolet radiation (5 mW·cm^{-2}, λ = 253.7 nm) for 900 s, a subsequent immersion of the samples in acetic acid bath for 300 s and a final O_2 plasma treatment for 120 s at 40 W.

Film Characterization

Scanning Electron Microscopy (SEM) analysis (Zeiss Supra 40 SEM) was used to acquire plan view images of the samples in order to evaluate the superficial ordering of the samples. the correlation length values ξ_{SEM} were extracted by software analysis of the SEM micrographs, following the standard procedure described in reference 2.

The morphological characterization at different depth in the BCP films was obtained by means of Grazing-Incidence Small-Angle X-ray Scattering (GISAXS) technique. The measurements were carried out in the SAXS beam line of the Elettra-Sincrotrone of Trieste (IT), using 8 keV photon energy. The horizontal and vertical widths of the beam focused at the sample position were 150 x 150 μm. The samples were placed on a computer controlled moving stage, allowing an accurate

alignment of the patterned area with respect to the incident beam direction. The GISAXS patterns were recorded on a 2D Pilatus 31M pixel detector system placed at a distance of 1750 mm from the sample. The intense incident and reflected beams were stopped by a 2 mm wide Al strip. To reduce air scattering the whole path of the incidence and scattered beam was under vacuum apart from the close vicinity of the sample. Data were fitted to pillars of circular cross section assembled in 2D hexagonal lattice.

All the samples were measured at α_c = 0.17° (grazing angle), chosen for the strongest scattering intensity and because it is the critical angle of incidence in our system. By varying the incident angle it is possible to tune the probed depth, thus the GISAXS technique offers the ability to probe the films from surface to buried interfaces. For this reason, measurements at different angles between α_c □□□□□ α_c + 0.11° have been also performed with steps of 0.01° (see Figure S1 and Figure S2 in Supporting Information) in order to extract information regarding the deeper portion of the BCP film. Below the critical angle the scattering depth is few nanometers, while it jumps abruptly to more than 1000 nm (i.e. higher ~~and more~~ than ~~all the samples~~ the thickness~~es~~ of the samples) immediately above the critical angle, as illustrated in Figure 1. Three different densities were assumed, and from the corresponding electron densities and X-rays energy (8 keV), the real and imaginary part of refraction index is calculated.[38-39] The real part influences the critical angle value, while the penetration, *i.e.* absorption, is controlled by the imaginary part. For X-rays, BCP is a soft material with low absorption and, once above the critical angle, the penetration depth extends easily to more than the film thickness.

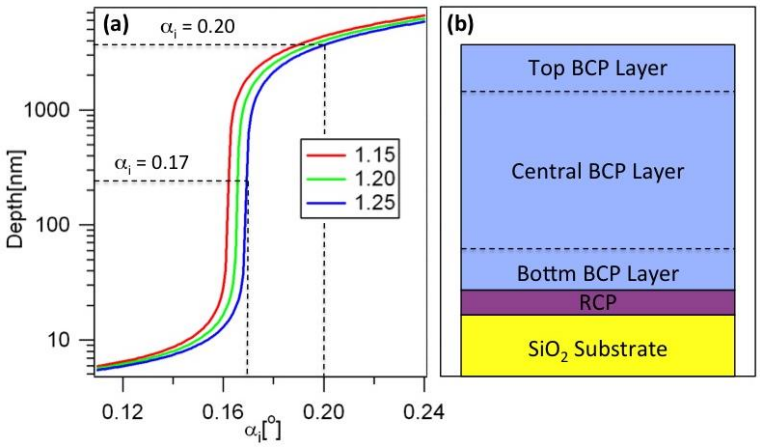

Figure 1: (a) Logarithmic scale graphic representing the calculated X-ray penetration depth inside the BCP matrix as a function of the incidence angle α_i for three different values of density, as indicated in the insert. The graphic is a zoomed to values around the critical angle α_c = 0.17. (b) Schematic representation of the cross-section of the samples, in which the SiO_2 substrate is represented in yellow, the RCP in purple and the BCP in blue. For the sake of clarity, the BCP film is also divided in three layers (top, central and bottom layers). The origin of these three layers will be treated along the manuscript.

Furthermore, we checked the sample homogeneity by repeating the GISAXS measurements in 10 different positions on the same sample: each time sample has been shifted horizontally in direction perpendicular to beam, while keeping the grazing angle constant. Since in general the correlation length calculated in different positions does not exceed a variation of 5 % as a function of the sample position, in the following experiments we will take into account the GISAXS performed in the central part of the samples.

RESULTS AND DISCUSSION

Thickness Variation

In order to examine the characteristics of the surface morphology a large set of samples having different thicknesses (h) ranging from 24 nm to 800 nm was prepared. The surface morphology

of the samples was systematically investigated by SEM. A ~~systematic~~ representative series of SEM plan view images is reported in Figures 2a-f. GISAXS analyses (Figure 2g) were performed on a selected set of samples to corroborate and complement SEM data. For $h \leq 100$ nm, the SEM images revealed a surface homogeneously composed of perpendicular oriented cylinders, organized in micrometric grains having different orientation. In this configuration, the only visible defects that modify the hexagonal arrangement consist in disclinations and dislocations (Figures 2a-b). On the other hand, by increasing the film thickness at $h \geq 194$ nm, we observed the presence some islands consisting of parallel oriented cylinders (Figure 2 c-d).

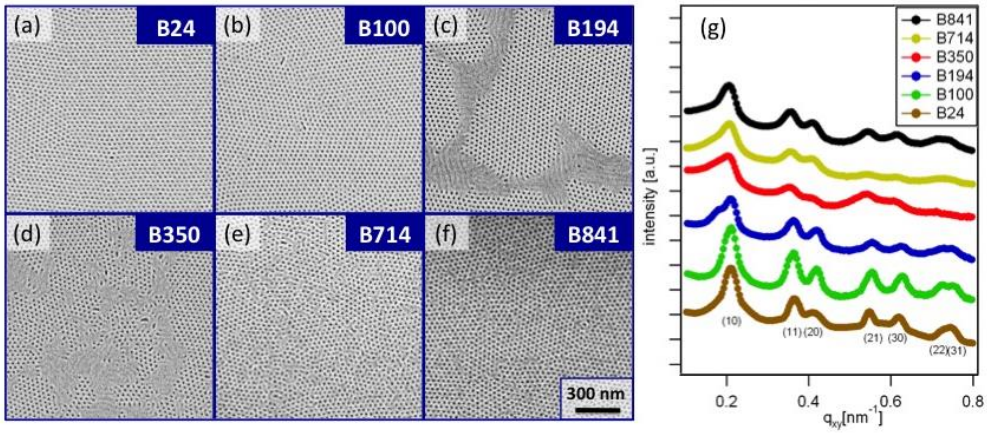

Figure 2: SEM plan view of the samples with different thickness: 24 nm (a), 100 nm (b), 194 nm (c), 350 nm (d) 714 nm (e) and 840 nm (f). The correspondent GISAXS profiles along q_{xy} at a constant q_z are also reported for all the samples (g).

Above a film thickness of h = 350 nm the dimension of the islands composed of parallel cylinders start to decrease, and few traces of parallel cylinders are visible in the thicker sample at $h \approx 800$ nm (Figures 2e-f). In order to analyze how the appearance of these parallel cylinders affects the long-range ordering of the perpendicular oriented cylinders, defined by the correlation length (ξ), we studied the evolution of ξ extracted from both SEM (Figure 3b), labeled as ξ_{SEM}, and GISAXS, labeled as ξ_{GISAXS} (Figure 3b). The general trend of ξ_{SEM} and ξ_{GISAXS} is similar.

Corresponding to low thickness, the film consists of a well-ordered structure. Then, a steep decrease of the lateral ordering of the perpendicular cylinders at the sample surface is observed. Finally, when the BCP reaches h = 841 nm, a slight increase in ξ occurs. The difference in the absolute values between ξ_{SEM} and ξ_{GISAXS} can be ascribed to the model-specific assumptions underlying the two distinct approaches. At a first analysis the decrease of ξ as a function of the film thickness parallels the occurrence of islands composed of parallel oriented cylinders in the top BCP layer, as demonstrated by the SEM micrographs reported in Figures 2c-d.

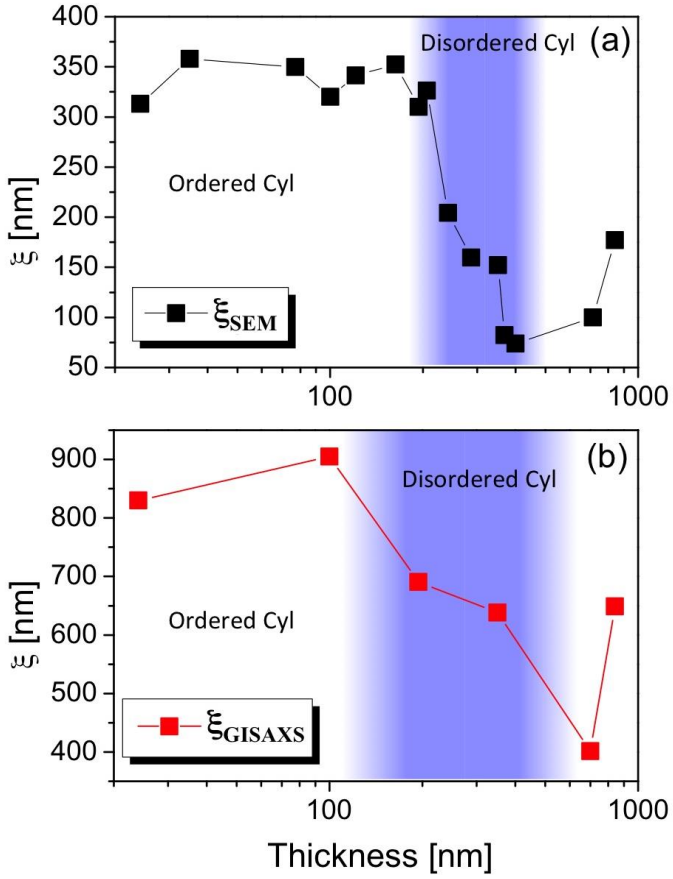

Figure 3: Correlation length ξ as a function of the BCP film thickness calculated by SEM (a) and by GISAXS analysis (b). The blue stripe indicates the zone in which we observed the reduction of the ordering of the perpendicular cylinders that can be ascribed to the appearance of parallel cylinders on the top surface of the samples. Outside the blue stripe a sensible reduction of the parallel cylinders is observed.

However, two different thresholds indicating that the starting point of the decrease of the lateral order of the nanodomains (pointed by the blue stripe in Figure 3a and 3b), can be found for ξ_{SEM} and ξ_{GISAXS} at 194 nm and 100 nm, respectively. Such a difference can be explained by noting that while the SEM analysis supplies information regarding the ordering of the nanodomains only at the surface of the samples, the ξ_{GISAXS} encompasses also the internal morphology of the samples. This is a first clue that underneath the top BCP layer composed of well-ordered cylinders some morphological changes are occurring.

The evolution of ξ as a function of the film thickness in samples processed by RTP annealing is very different compared to that reported for the PS-*b*-PMMA systems with the same M_n but treated in furnaces or hotplates, for longer annealing. In the latter cases, a linear increase in ξ as h increases has been observed in samples with thickness up to $h \approx 600$ nm, while in our previous experiments no linear trend can be observed.[2] To further deep into the cause of the non-linear dependence of ξ on the film thickness in samples RTP treated, an in-depth analysis of the BCP films is needed. With this purpose, the intensity profiles along q_{xy} of the GISAXS patterns (Figure 4a) have been extracted for all the samples under analysis at constant q_z for different incidence angles (Figure S1), corresponding to the critical angle α_c (empty circles) and at a superior angle α_c+0.1° (solid circles).

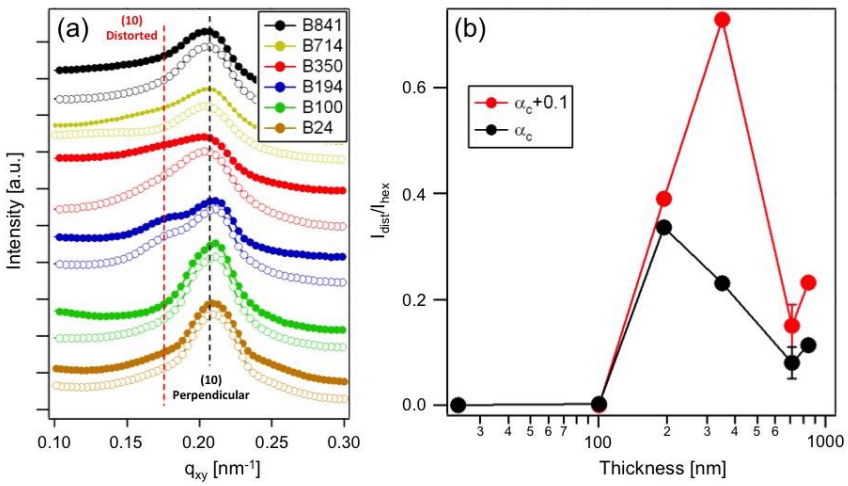

Figure 4: (a) GISAXS profiles cut at constant q_z taken at two different incidence angles α_c (empty circles) and α_c+0.1º (solid circles) around the (10) peak on samples with different thickness between the B24 and the B840. (b) Ratio between the intensity related to the distorted I_{dist} and the hexagonal cylinders I_{hex} measured at α_c (red circles) and α_c+0.1º (blue circles).

According to Figure 1, at the critical angle α_c, the GISAXS is mostly influenced by the orientation and ordering of the cylinders placed on first 200 nm of the surface of the sample. Instead, the GISAXS analysis performed at α_c+0.1° provides insights regarding the disposition of the cylinders along the whole thickness of the film.

For B24 and B100 only a single and well-defined peak is visible at both incidence angles (see brown and green lines in Figure 4a), corresponding to the first order (10) of hexagonally packed perpendicular cylinders. However, by increasing h, a second peak emerges at minor q_{xy} with lower intensity than the first order peak of the hexagonally arranged cylinders. In order to unveil the origin of this second peak simulations have been performed considering three possible configurations of the system, as described in Figure S3: (a) perpendicular oriented cylinders, (b) cylinders disposed in both parallel and perpendicular orientation and (c) a superficial layer composed by perpendicular cylinders over a zone in which the nanostructures are oriented in all

possible directions (labeled as distorted cylinders). In all the configurations a layer of perpendicularly oriented cylinder is introduced at the polymer/substrate interface where the RCP brush layer is expected to neutralize the surface avoiding any kind of preferential wetting. The presence of this layer of perpendicular cylinders has already been experimentally demonstrated in previous works. According to the simulations, the second peak in the GISAXS spectra of Figure 4a can be associated to partial loss of the perpendicular orientation of the nanostructures, due to a distortion of their orientation from perpendicular to parallel with respect to the substrate. This result is perfectly consistent with experimental results obtained on similar BCP systems[40]. The q_z cuts of the GISAXS patterns taken at different incidence angles (Figure S2) suggest that the distortion process of the cylinders along the film section is a gradual process.

To extract additional information regarding the distribution of the orientations of the cylinders along the depth of the BCP films, we analyzed the ratio I_{dist}/I_{hex} of intensity of the peak corresponding to the perpendicular oriented cylinders (I_{hex}) and that distorted ones (I_{dist}). The results of this calculation are illustrated in Figure 4b for the two incidence angles α_c (black squares) and α_c+0.1° (red circles). The ratio I_{dist}/I_{hex} of the samples B24 and B100 is approximately zero for both incidence angles, confirming the presence of perpendicular oriented cylinders only, spanning the top of the BCP film without any distortion. In the case of B194, the value of I_{dist}/I_{hex} starts to increase, reaching the value of 0.35. By further increasing the film thickness to 350 nm, a difference between the ratio calculated at the two angles α_c and α_c+0.1° is observed. A value of I_{dist}/I_{hex} = 0.2 is obtained at α_c while at α_c+0.1° a ratio of I_{dist}/I_{hex} = 0.7 is determined. In this case, it is clear that the amount of parallel oriented cylinders increases in the central BCP layer with respect to the top BCP layer. Finally, for B714 and B840 the intensity

ratio calculated at the different angles drops to ~ 0.1 at α_c and ~ 0.2 when moving to α_c+0.1°, indicating a huge reduction of the number of parallel oriented cylinders in the thickest sample.

For the two latter samples, the data reported in Figure 4b, along with the SEM micrographs shown in Figure 2e-f representing the surface morphology of the samples, indicate that the orientation changing process of the cylinders is preferentially taking place in the central BCP layer rather than in the top BCP layer, that is mostly composed of a layer of perpendicular oriented cylinders. To estimate the thickness of the superficial layer consisting of perpendicular cylinders, and consequently the depth at which the distortion of the cylinders occurs inside the film, one possible method is the analysis of the intensity modulations of the GISAXS pattern taken along the q_z direction in correspondence of the (10) rods. This intensity modulation is due to the formation of layers having different average refractive indexes. Since the selective removal of the PMMA described in the experimental section is effective only to empty the perpendicular oriented cylinders, it is possible to observe the interfaces composed of cylinders with different orientation (empty perpendicular cylinders and full parallel cylinders). By fitting the thickness related intensity oscillations correspondent to the samples B24 and B100 (purple and blue curves in Figure 5) we obtained values of 26 nm and 105 nm respectively. Within the experimental error these results perfectly matches with the nominal thickness of the as deposited films. Therefore, we can conclude that the thinner samples consist in a single layer of perpendicular cylinders spanning completely along the top, central and bottom BCP layers. On the other hand, in the vertical profile of samples B194 and B350 only a smooth modulation is visible and the precise determination of a layer thickness is very difficult to obtain. This result indicates that in the thickness range between 194 nm and 350 nm the BCP films are composed of cylinders with no preferential direction. Finally, for the sample B840, we observe the formation

of a top BCP layer having thickness of 54 nm composed of perpendicular cylinders. This thickness value is in good agreement with that obtained by neutron reflectivity on ~~similar~~ deuterated PS-b-PMMA BCPs.[3]

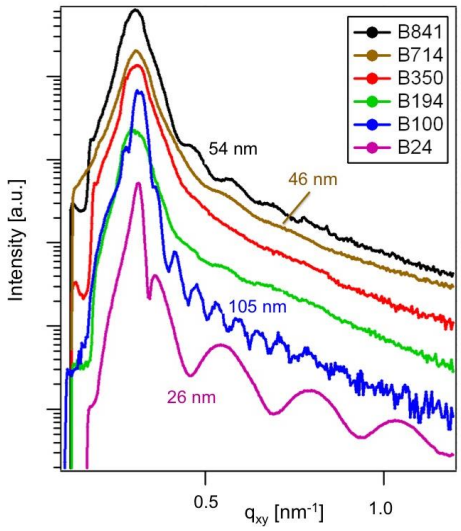

Figure 5: Vertical cross section along the (10) rods extracted from the GISAXS patterns of the analyzed samples at different thickness.

The values of ξ□□□□□□ reported in Figure 3 are mostly influenced by the long range ordering of the cylinders perpendicularly oriented to the surface of the BCP film. The estimation of ξ for the parallel oriented cylinders is much complicate to perform, since the correspondent GISAXS peak is convoluted with the (10) peak characteristic of the perpendicular cylinders, as shown in Figure 4a. However, when scattering at α_c is subtracted from the scattering at α_c+0.1°, the signal from perpendicular oriented cylinders present on the surface of the film is suppressed, while the signal coming from the central and bottom BCP layers is enhanced. Figures 6a-d illustrated the individual contribution of the scattering from the horizontal cylinders lying deep in the film. After the subtraction process, the signal related to the sample B100 does not show the presence of any additional peaks ascribable to the parallel oriented cylinders (Figure 6a).

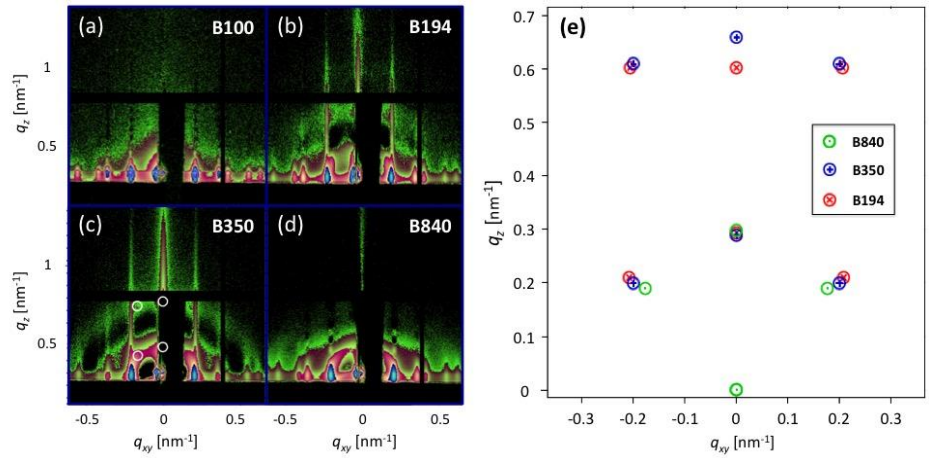

Figure 6: GISAXS pattern resulting from the subtraction of the patterns at α_c and α_c+0.1° for samples with thickness of (a) 100 nm, (b) 194 nm, (c) 350 nm and (d) 841 nm. (e) Representation of the Bragg spots position for the samples B840 (green circles), B350 (blue circles) and B194 (red circles).

On the contrary, in Figures 6b-d the appearance of isotropic ring like scattering in the subtracted GISAXS patterns of samples thicker than 100 nm, suggests that the transition of the cylinders between perpendicular and parallel is not a sharp process, but the orientation gradually changes along the film section. Such rings are more pronounced in B194 and B350 than in B840. This is consistent with the disappearance of parallel cylinders on the surface of sample B840 observed in the SEM analysis, and with the simultaneous formation of a 54 nm thick superficial layer formed by perpendicular oriented cylinders in this specific sample. In all these samples, the GISAXS analysis revealed that the hexagonal ordering of the parallel cylinders also propagates in the vertical direction with respect to the substrate. This is clear by looking at the diffuse spots at positions indicated with circles in Figures 6c and 6e. The plot of the Bragg positions suggests that the structure slightly differs in the samples. Moreover, the positions of the spots are quite different from those of a regular hexagonal structure. Due to the formation of defective structures, the Bragg spots are broadened into diffuse ring. In sample B840, only the first order

ring is present (green circles in Figure 6e), while in B350 and B194 (blue and red circles in Figure 6e, respectively) also the second order is visible. The thinner samples ($h \leq 100$ nm) display only the central diffuse signal ascribed to the form factor of the cylinders whereas the signal from horizontally placed cylinders is completely suppressed.

Time evolution of the BCP ordering

In order to study the evolution of the buried layers composed of parallel and perpendicular oriented cylinders as a function of the annealing time, a second set of samples has been prepared varying the annealing time between $t_a = 0$ s (not annealed sample) and $t_a = 900$ s and keeping the film thickness constant at $h \approx 700$ nm. This thickness was chosen because it corresponds to the minimum value of the long-range ordering of the perpendicular cylinders that indicating that this system presents the highest degree of disorder. Following the previously described procedure, the GISAXS analysis of the samples, treated for different t_a, was performed by varying the grazing angles between α_c and $\alpha_c + 0.1°$ with a step of 0.01°, thus selecting a different thickness inside the film. As expected, the GISAXS performed on the not annealed sample does not show the presence of vertical streaks due to aligned perpendicular cylinders (Figure 7). The only visible pattern is composed of a strong ring-like scattering, which is not circular but rather elongated in vertical direction.

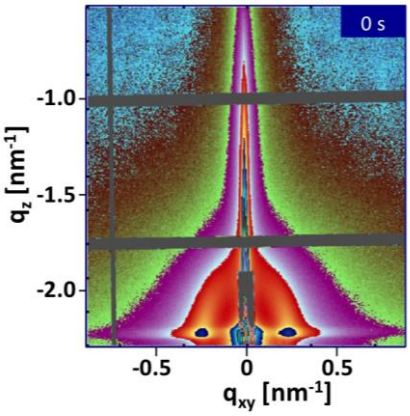

Figure 7: GISAXS pattern corresponding to the not annealed sample (t = 0 s).

On the other hand, the annealed samples have two different kinds of SAXS signals as observed in Figures 8a-e, namely the ring like scattering (centered at the incoming beam direction), and the scattering along q_{xy} due to a two-dimensional hexagonal lattice composed of perpendicular oriented cylinders. The intensity of the Bragg peaks, especially at higher orders, can be directly associated to the defect concentration in the BPC film. The defect reduction as a function of the annealing time is even clearer by looking at the SEM micrographs reported in Figures 8f-l that represent the superficial morphology of the samples. By extracting the horizontal cross section of the GISAXS spectra reported in Figures 8a-e, it is possible to have some insight regarding the long range ordering of the perpendicular cylinders (Figure 9a).

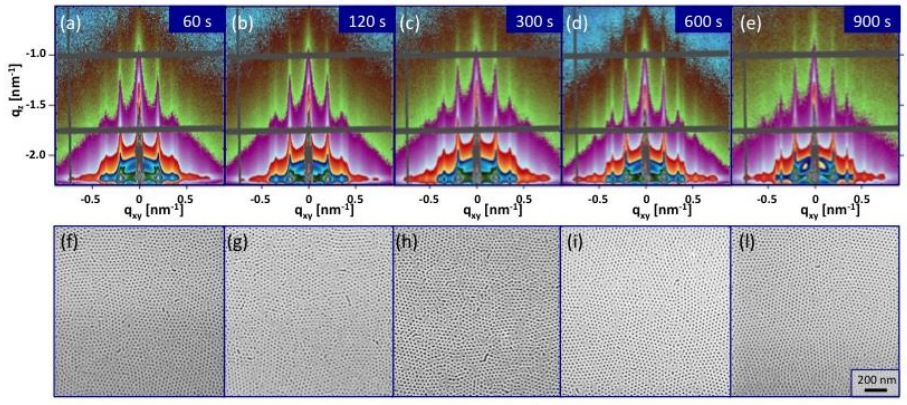

Figure 8: (a-e) GISAXS patterns and (f-l) SEM micrographs taken on 700 nm thick samples treated at 270 °C for different annealing times ranging between 0 s and 900 s.

As can be seen in Figure 9a, the defect concentration is reduced with increasing annealing time, since (11) and (20) peaks are steadily gaining intensity going from t_a = 60 to t_a = 900 s. On the other hand, the vertical cross section along the (10) rods extracted from the GISAXS patterns (Figure 9b) suggests that the thickness of the superficial layer composed of perpendicular cylinders is not changing significantly as a function of the annealing time. The thickness of this layer slowly decreases from 48 nm for a 30 s treatment to 40 nm after a 900 s treatment (Figure 9c).

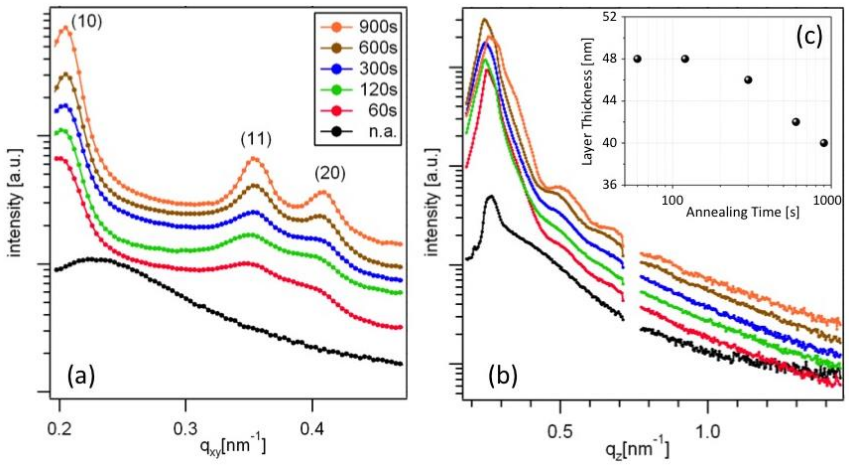

Figure 9: (a) GISAXS intensity of the scattering in horizontal direction (q_{xy}) for samples treated at different t_a. (b) Intensity along the first Bragg streak vs q_z. (c) Superficial layer thickness as a function of the annealing time.

In order to quantify the increase in the lateral ordering of the perpendicular cylinders at the sample surface as t_a increases, ξ was extracted from both SEM and GISAXS at different incident angles and the growth exponent ϕ was calculated. The value of ϕ extracted by the SEM images

(labeled as ϕ_{SEM} in Figure 10) is higher than ϕ_{GISAXS} at all the different incidence angles. This indicates that the ordering kinetics is faster in the top BCP layer than in the central BCP later. These values, obtained on samples having $h \approx 700$ nm, are compatible with the growth exponent characteristic of the *slow coarsening* regime that has already been reported for the same PS-*b*-PMMA system in samples with $h \approx 30$ nm treated at $T_a = 270$ °C (*i.e.* $\phi_{SLOW} = 0.19$).[41] The comparison of these data with those in the literature for 30 nm thick PS-*b*-PMMA films points out that the thermal energy that long annealing treatment supplies to the BCP system is used preferentially to increase the in plane ordering in the top BCP layer rather than to extend the depth of the cylinders along the film.

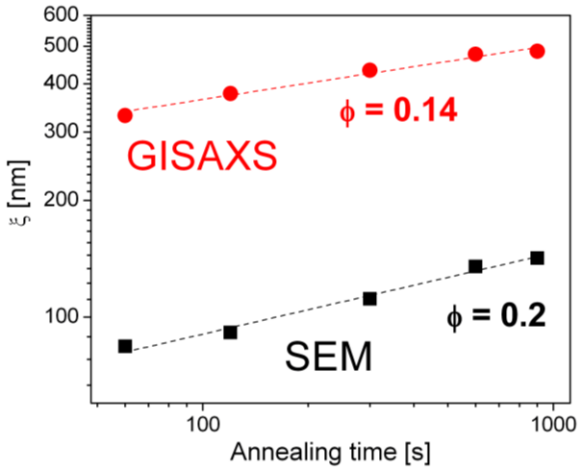

Figure 10: ξ_{SEM} and ξ_{GISAXS} calculated for samples annealed at different t_a between 60 s and 900 s.

Similarly to what observed in the previous experiments, the vertical intensity distribution along the first Bragg peak for all the samples annealed at different t_a presents some faint oscillations due to the formation of a superficial layer composed of perpendicular oriented cylinders (Figure 10). The thickness of such layer increases with increasing t_a up to a maximum value of 35 nm, obtained at $t_a = 900$ s. The relatively low intensity of these fringes is either due to a very low

contrast in electron density between the top and bottom layers, and/or to an inhomogeneous thickness along the probed part of the sample.

DISCUSSION

The general picture of the morphological structures of the nanodomains in thick PS-*b*-PMMA films treated at high temperatures in the RTP machine is schematically illustrated in Figure 11. As previously observed in similar systems,[42] the perpendicular orientation of the cylinders starts propagating simultaneously from the upper interface (Air-BCP) and the lower interface (modified SiO_2-BCP). It was also demonstrated that there is a thickness limit (opp limiting thickness) above which the ordering dynamics of the two interfaces are "decoupled". Below such thickness limit, there is connectivity between the two interfaces and the BCP film is as a single and homogeneous layer composed of perpendicular oriented cylinders spanning the entire thickness. When the sample is RTP processed at high temperature (T_a = 270 °C) and for short processing time (t_a = 300 s), this limit thickness is above h = 100 nm (Figure 11a). This corresponds to the limit at which these PS-*b*-PMMA films can be used for lithographic applications. More precisely, previous experiments[41] locate such limit around h = 160 nm. Then, by further increasing the BCP thickness up to h = 700 nm, a reduction of the lateral ordering of the perpendicular cylinders at the sample surface and the formation of bent and parallel oriented cylinders in both the surface and the internal part of the film are observed. In the thickness range $160 < h < 700$ (Figure 11b), the top, the central and the bottom BCP layers act as individual and uncorrelated layers in which all the orientations of the cylinders are allowed. In the top BCP layer the perpendicular orientation prevails as demonstrated by the SEM micrographs of Figure

2c-d and by the intensity ratios reported in Figure 4b. Considering the formation of the perpendicular cylinders in the bottom BCP layer previously reported in literature and the predominance of the perpendicular orientation on the top BCP layer, we can hypothesize that in the thickness range $160 < h < 700$ the BCP film undergoes to a sort of "influence regime". In this regime the perpendicular cylinders, formed in the top BCP layer, gradually tilt in the central BCP layer to join the perpendicular cylinders formed at the bottom BCP layer. Even the increase in the annealing time does not lead the cylinders of the top BCP layer to perpendicularly reach those in the bottom BCP layer, since they seem to be always subjected to a bending process. Finally, for $h \geq 700$ nm, the previously described "influence regime" is no more observed (Figure 11c). The two interfaces are completely decoupled and a top BCP layer of approximately 50-60 nm of perpendicular oriented cylinders is formed while the inner part of the film is characterized by the presence of cylinders that are parallel oriented to the substrate. It is interesting to note that the thickness of the superficial layer of the B840 is approximately half the value indicated in our previous work as the thickness limit for the complete propagation of the perpendicular cylinders through the whole film. This result suggests that the top and the bottom layers equally contribute to the formation of the described "influence regime". Finally, the correlation growth exponents calculated at $h \approx 700$ nm indicate that the self-assembly process follows a dynamics similar to that reported for the thin films of PS-*b*-PMMA deposited directly over the random copolymer.

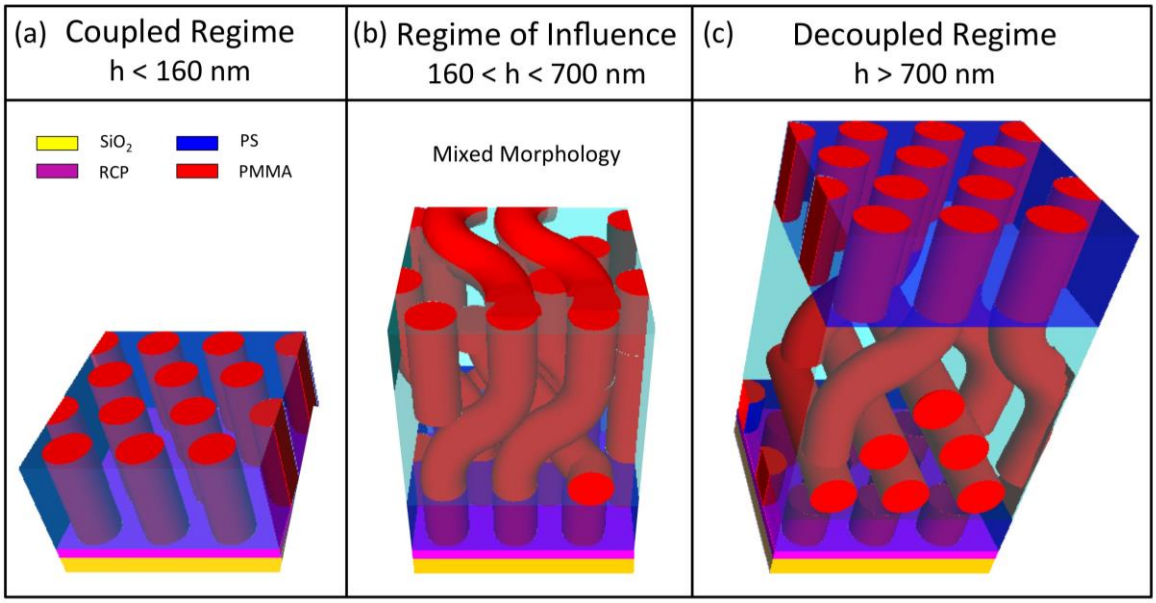

Figure 11: Scheme of the morphological structures in PS-*b*-PMMA films with thickness comprised between 24 and 800 nm. The three configurations of coupled regime (a), influence regime (b), and decoupled regime (c) are also indicated.

CONCLUSIONS

In this work we systematically studied by GISAXS the orientation and ordering mechanism in thick BCP films processed at high temperatures. Three distinct regimes as a function of the film thickness were observed, in which the self-assembly process lead to the formation of buried layers featuring different orientations of the PMMA cylinders. In the first regime ($h \leq 160$ nm), the cylinders span perpendicular along the whole film. In the second regime ($160 < h < 700$ nm), the presence of a mixed morphology consisting in parallel, perpendicular, and pended cylinders was observed at both the upper surface and in the internal part of the film. Finally, in the third regime ($h \geq 700$ nm), the behavior of the upper surface is decoupled from that of the internal part

of the film. In this case, the formation of a superficial layer mostly composed of perpendicular cylinders was detected while in the inner no preferential orientation seem to be present. The thickness of such superficial layer is about ~ 50 nm and cannot be further increased by longer thermal treatments. Indeed, by keeping the film thickness constant and increasing the annealing time, an increase in the lateral ordering of the cylinders was observed while the thickness of the upper layer remains constant. All the experimental observations reported in this work lead to the conclusion that the superficial ordering of the nanostructure is strongly influenced by the in-depth arrangement of the nanodomains.

ACKNOWLEDGEMENTS

This work has been carried out in the framework of the project 14IND01 "3DMetChemIT", founded by the EMPIR programme, co-financed by the Participating States and from the European Union's Horizon 2020 research and innovation programme.

REFERENCES

(1) Sunday, D. F.; Hammond, M. R.; Wang, C.; Wu, W. L.; Delongchamp, D. M.; Tjio, M.; Cheng, J. Y.; Pitera, J. W.; Kline, R. J. Determination of the Internal Morphology of Nanostructures Patterned by Directed Self Assembly. *ACS Nano* **2014**, *8* (8), 8426–8437.

(2) Ji, S.; Liu, C.; Liao, W.; Fenske, A. L.; Craig, G. S. W.; Nealey, P. F. Domain Orientation and Grain Coarsening in Cylinder-Forming Poly (Styrene-b-Methyl Methacrylate) Films. *Macromolecules* **2011**, 4291–4300.

(3) Zhang, X.; Berry, B. C.; Yager, K. G.; Kim, S.; Jones, R. L.; Satija, S.; Pickel, D. L.; Douglas, J. F.; Karim, A. Surface Morphology Diagram for Cylinder-Forming Block Copolymer Thin Films. *ACS Nano* **2008**, *2* (11), 2331–2341.

(4) Phillip, W. A.; O'neill, B.; Rodwogin, M.; Hillmyer, M. A.; Cussler, E. L. Self-Assembled Block Copolymer Thin Films as Water Filtration Membranes. *ACS Appl. Mater.*

Interfaces **2010**, *2* (3), 847–853.

(5) Jackson, E. A.; Hillmyer, M. A. Nanoporous Membranes Derived from Block Copolymers: From Drug Delivery to Water Filtration. *ACS Nano* **2010**, *4* (7), 3548–3553.

(6) Lee, A.; Darling, S. B. Membrane Materials for Water Purification: Design, Development, and Application. *Environ. Sci. Water Res. Technol.* **2016**, *2* (1), 17–42.

(7) Yang, S. Y.; Ryu, I.; Kim, H. Y.; Kim, J. K.; Jang, S. K.; Russell, T. P. Nanoporous Membranes with Ultrahigh Selectivity and Flux for the Filtration of Viruses. *Adv. Mater.* **2006**, *18* (6), 709–712.

(8) Orilall, M. C.; Wiesner, U. Block Copolymer Based Composition and Morphology Control in Nanostructured Hybrid Materials for Energy Conversion and Storage: Solar Cells, Batteries, and Fuel Cells. *Chem. Soc. Rev.* **2011**, *40* (2), 520–535.

(9) Bouchet, R.; Maria, S.; Meziane, R.; Aboulaich, A.; Lienafa, L.; Bonnet, J.-P.; Phan, T. N. T.; Bertin, D.; Gigmes, D.; Devaux, D.; Denoyel, R.; Armand, M. Single-Ion BAB Triblock Copolymers as Highly Efficient Electrolytes for Lithium-Metal Batteries. *Nat. Mater.* **2013**, *12* (5), 452–457.

(10) Sing, C. E.; Zwanikken, J. W.; Olivera de la Cruz, M. Electrostatic Control of Block Copolymer Morphology. *Nat. Mater.* **2014**, *13* (7), 694–698.

(11) Guo, C.; Lin, Y. H.; Witman, M. D.; Smith, K. A.; Wang, C.; Hexemer, A.; Strzalka, J.; Gomez, E. D.; Verduzco, R. Conjugated Block Copolymer Photovoltaics with near 3% Efficiency through Microphase Separation. *Nano Lett.* **2013**, *13* (6), 2957–2963.

(12) Darling, S. B. Block Copolymers for Photovoltaics. *Energy Environ. Sci.* **2009**, *2* (12), 1266.

(13) Topham, P. D.; Parnell, A. J.; Hiorns, R. C. Block Copolymer Strategies for Solar Cell Technology. *J. Polym. Sci. Part B Polym. Phys.* **2011**, *49* (16), 1131–1156.

(14) Kim, E.; Kim, W.; Lee, K. H.; Ross, C. A.; Son, J. G. A Top Coat with Solvent Annealing Enables Perpendicular Orientation of Sub-10 Nm Microdomains in Si-Containing Block Copolymer Thin Films. *Adv. Funct. Mater.* **2014**, *24* (44), 6981–6988.

(15) Kim, J. M.; Kim, Y.; Park, W. I.; Hur, Y. H.; Jeong, J. W.; Sim, D. M.; Baek, K. M.; Lee, J. H.; Kim, M.-J.; Jung, Y. S. Eliminating the Trade-Off between the Throughput and Pattern Quality of Sub-15 Nm Directed Self-Assembly via Warm Solvent Annealing. *Adv. Funct. Mater.* **2015**, *25*, 306–315.

(16) Xu, T.; Kim, H.-C.; DeRouchey, J.; Seney, C.; Levesque, C.; Martin, P.; Stafford, C. M.; Russell, T. P. The Influence of Molecular Weight on Nanoporous Polymer Films. *Polymer (Guildf).* **2001**, *42* (21), 9091–9095.

(17) Boker, A.; Elbs, H.; Hansel, H.; Knoll, A.; Ludwigs, S.; Zettl, H.; Zvelindovsky, A. V.; Sevink, G. J. A.; Urban, V.; Abetz, V.; Mu; Ller, A. H. E.; Krausch, G. Electric Field Induced Alignment of Concentrated Block Copolymer Solutions. *Macromolecules* **2003**, *36* (21), 8078–8087.

(18) Mansky, P.; Liu, Y.; Russell, T. P.; Hawker, C. Controlling Polymer-Surface Interactions with Random Copolymer Brushes. *Science (80-.).* **1997**, *275* (5305), 1458–1460.

(19) Tseng, Y. C.; Peng, Q.; Ocola, L. E.; Elam, J. W.; Darling, S. B. Enhanced Block Copolymer Lithography Using Sequential Infiltration Synthesis. *J. Phys. Chem. C* **2011**, *115* (36), 17725–17729.

(20) Peng, Q.; Tseng, Y. C.; Darling, S. B.; Elam, J. W. Nanoscopic Patterned Materials with Tunable Dimensions via Atomic Layer Deposition on Block Copolymers. *Adv. Mater.* **2010**, *22* (45), 5129–5133.

(21) Jacobs, A. G.; Jung, B.; Jiang, J.; Ober, C. K.; Thompson, M. O. Control of Polystyrene-Block-Poly(methyl Methacrylate) Directed Self-Assembly by Laser-Induced Millisecond Thermal Annealing. *J. Micro/Nanolithography, MEMS, MOEMS* **2015**, *14* (3), 31205.

(22) Ferrarese Lupi, F.; Giammaria, T. J.; Ceresoli, M.; Seguini, G.; Sparnacci, K.; Antonioli, D.; Gianotti, V.; Laus, M.; Perego, M. Rapid Thermal Processing of Self-Assembling Block Copolymer Thin Films. *Nanotechnology* **2013**, *24* (31).

(23) Ferrarese Lupi, F.; Giammaria, T. J.; Seguini, G.; Vita, F.; Francescangeli, O.; Sparnacci, K.; Antonioli, D.; Gianotti, V.; Laus, M.; Perego, M. Fine Tuning of Lithographic Masks through Thin Films of PS-B -PMMA with Different Molar Mass by Rapid Thermal Processing. *ACS Appl. Mater. Interfaces* **2014**, *6* (10), 7180–7188.

(24) Seguini, G.; Giammaria, T. J.; Ferrarese Lupi, F.; Sparnacci, K.; Antonioli, D.; Gianotti, V.; Vita, F.; Placentino, I. F.; Hilhorst, J.; Ferrero, C.; Francescangeli, O.; Laus, M.; Perego, M. Thermally Induced Self-Assembly of Cylindrical Nanodomains in Low Molecular Weight PS-B-PMMA Thin Films. *Nanotechnology* **2014**, *25* (4), 45301.

(25) Ceresoli, M.; Ferrarese Lupi, F.; Seguini, G.; Sparnacci, K.; Gianotti, V.; Antonioli, D.; Laus, M.; Boarino, L.; Perego, M. Evolution of Lateral Ordering in Symmetric Block Copolymer Thin Films upon Rapid Thermal Processing. *Nanotechnology* **2014**, *25* (27).

(26) Ferrarese Lupi, F.; Giammaria, T. J.; Seguini, G.; Ceresoli, M.; Perego, M.; Antonioli, D.; Gianotti, V.; Sparnacci, K.; Laus, M. Flash Grafting of Functional Random Copolymers for Surface Neutralization. *J. Mater. Chem. C* **2014**, *2* (25), 4909–4917.

(27) Perego, M.; Ferrarese Lupi, F.; Ceresoli, M.; Giammaria, T. J.; Seguini, G.; Enrico, E.; Boarino, L.; Antonioli, D.; Gianotti, V.; Sparnacci, K.; Laus, M. Ordering Dynamics in Symmetric PS-B-PMMA Diblock Copolymer Thin Films during Rapid Thermal

Processing. *J. Mater. Chem. C* **2014**, *2* (32), 6655–6664.

(28) Kim, S. H.; Misner, M. J.; Russell, T. P. Solvent-Induced Ordering in Thin Film Diblock Copolymer/homopolymer Mixtures. *Adv. Mater.* **2004**, *16* (23–24), 2119–2123.

(29) Phillip, W. A.; Hillmyer, M. A.; Cussler, E. L. Cylinder Orientation Mechanism in Block Copolymer Thin Films upon Solvent Evaporation. *Macromolecules* **2010**, *43* (18), 7763–7770.

(30) Cui, G.; Fujikawa, M.; Nagano, S.; Shimokita, K.; Miyazaki, T.; Sakurai, S.; Yamamoto, K. Macroscopic Alignment of Cylinders via Directional Coalescence of Spheres along Annealing Solvent Permeation Directions in Block Copolymer Thick Films. *Macromolecules* **2014**, *47* (17), 5989–5999.

(31) Paradiso, S. P.; Delaney, K. T.; García-Cervera, C. J.; Ceniceros, H. D.; Fredrickson, G. H. Block Copolymer Self Assembly during Rapid Solvent Evaporation: Insights into Cylinder Growth and Stability. *ACS Macro Lett.* **2014**, *3* (1), 16–20.

(32) Zhang, J.; Posselt, D.; Smilgies, D. M.; Perlich, J.; Kyriakos, K.; Jaksch, S.; Papadakis, C. M. Lamellar Diblock Copolymer Thin Films during Solvent Vapor Annealing Studied by Gisaxs: Different Behavior of Parallel and Perpendicular Lamellae. *Macromolecules* **2014**, *47* (16), 5711–5718.

(33) Ferrarese Lupi, F.; Giammaria, T. J.; Seguini, G.; Laus, M.; Enrico, E.; De Leo, N.; Boarino, L.; Ober, C. K.; Perego, M. Thermally Induced Orientational Flipping of Cylindrical Phase Diblock Copolymers. *J. Mater. Chem. C* **2014**, *2* (12), 2175–2182.

(34) Ferrarese Lupi, F.; Aprile, G.; Giammaria, T. J.; Seguini, G.; Zuccheri, G.; De Leo, N.; Boarino, L.; Laus, M.; Perego, M. Thickness and Microdomain Orientation of Asymmetric PS-B-PMMA Block Copolymer Films Inside Periodic Gratings. *ACS Appl. Mater. Interfaces* **2015**, *7* (42), 23615–23622.

(35) Biswas, M.; Ren, J.; Suh, H. S.; Darling, S. B.; Liddle, J. A.; Elam, J. W.; Pablo, J. J. De; Zaluzec, N. J.; Nealey, P. F. Characterizing the Three-Dimensional Structure of Block Copolymers via Sequential In Fi Ltration Synthesis and Scanning Transmission Electron. *ACS Nano* **2015**, *9* (5), 5333–5347.

(36) Maret, M.; Tiron, R.; Chevalier, X.; Gergaud, P.; Gharbi, A.; Lapeyre, C.; Pradelles, J.; Jousseaume, V.; Fleury, G.; Hadziioannou, G.; Boudet, N.; Navarro, C. Probing Self-Assembly of Cylindrical Morphology Block Copolymer Using in Situ and Ex Situ Grazing Incidence Small-Angle X-Ray Scattering: The Attractive Case of Graphoepitaxy. *Macromolecules* **2014**, *47* (20), 7221–7229.

(37) Sparnacci, K.; Antonioli, D.; Gianotti, V.; Laus, M.; Ferrarese Lupi, F.; Giammaria, T. J.; Seguini, G.; Perego, M. Ultrathin Random Copolymer-Grafted Layers for Block

Copolymer Self-Assembly. *ACS Appl. Mater. Interfaces* **2015**, *7* (20), 10944–10951.

(38) Muller-Buschbaum, P. GISAXS and GISANS as Metrology Technique for Understanding the 3D Morphology of Block Copolymer Thin Films. *Eur. Polym. J.* **2015**.

(39) Saito, I.; Miyazaki, T.; Yamamoto, K. Depth-Resolved Structure Analysis of Cylindrical Microdomain in Block Copolymer Thin Film by Grazing-Incidence Small-Angle X-Ray Scattering Utilizing Low-Energy X-Rays. *Macromolecules* **2015**, *48* (22), 8190–8196.

(40) Samant, S.; Strzalka, J.; Yager, K. G.; Kisslinger, K.; Grolman, D.; Basutkar, M.; Salunke, N.; Singh, G.; Berry, B.; Karim, A. Ordering Pathway of Block Copolymers under Dynamic Thermal Gradients Studied by in Situ GISAXS. *Macromolecules* **2016**, *49* (22), 8633–8642.

(41) Ferrarese Lupi, F.; Giammaria, T. J.; Volpe, F. G.; Lotto, F.; Seguini, G.; Pivac, B.; Laus, M.; Perego, M. High Aspect Ratio PS-B-PMMA Block Copolymer Masks for Lithographic Applications. *ACS Appl. Mater. Interfaces* **2014**, *6* (23), 21389–21396.

(42) Han, E.; Stuen, K. O.; Leolukman, M.; Liu, C. C.; Nealey, P. F.; Gopalan, P. Perpendicular Orientation of Domains in Cylinder-Forming Block Copolymer Thick Films by Controlled Interfacial Interactions. *Macromolecules* **2009**, *42* (13), 4896–4901.